applied sciences

MDPI

Article

An Evaluation of the Usability of Argon Plasma-Treated Bacterial Cellulose as a Carrier for Controlled Releases of Glycoside Hydrolases $PelA_h$ and $PslG_h$, Which Are Able to Eradicate Biofilm

Magdalena Chareza [1], Ewa Ekiert [2], Dariusz Moszyński [2], Mariusz Madej [3], Magdalena Jędrzejczak-Silicka [4] and Radosław Drozd [1,*]

[1] Department of Microbiology and Biotechnology, Faculty of Biotechnology and Animal Husbandry, West Pomeranian University of Technology in Szczecin, 45 Piastow Avenue, 71-311 Szczecin, Poland; magdalena.szymanska@zut.edu.pl
[2] Department of Inorganic Chemical Technology and Environment Engineering, Faculty of Chemical Technology and Engineering, West Pomeranian University of Technology in Szczecin, 42 Piastow Avenue, 71-065 Szczecin, Poland; ewa.dabrowa@zut.edu.pl (E.E.); dariusz.moszynski@zut.edu.pl (D.M.)
[3] Department of Microbiology, Faculty of Biochemistry, Biophysics, and Biotechnology, Jagiellonian University, Gronostajowa 7, 30-387 Kraków, Poland; mariusz.madej@uj.edu.pl
[4] Laboratory of Cytogenetics, West Pomeranian University of Technology in Szczecin, Klemensa Janickiego 29, 71-270 Szczecin, Poland; magdalena.jedrzejczak@zut.edu.pl
* Correspondence: rdrozd@zut.edu.pl; Tel.: +48-517456798

Abstract: Bacterial cellulose is a unique biopolymer that has found numerous biomedical applications, such as being an excellent wound-dressing material or a carrier for delivering active compounds. The purpose of this study was to analyze the ability of modified bacterial cellulose (BC) using low-pressure Ar plasma to control the release of glycoside hydrolases with antibiofilm activity, namely $PelA_h$ and $PslG_h$, from *Pseudomonas aeruginosa*. The chemical composition and morphology of the BC surfaces were characterized using photoelectron spectroscopy (XPS), Fourier transform infrared spectroscopy (FTIR), and scanning electron microscopy (SEM). The analyses revealed significant changes in the chemical composition of the BC surface due to the introduction of charged functional groups and the conversion of its well-ordered structure into a more amorphous form. The release profiles of enzymes from both forms of the carrier were different and depended on their structural properties. However, a significant impact of BC modification on protein release behavior from the carrier was observed only for $PslG_h$. Both enzymes, when immobilized on pristine and argon plasma-modified BC, retained their ability to effectively reduce biofilm levels, similarly to their soluble form. Ar plasma-modified BC with immobilized specific hydrolases can be used as an effective tool for inhibiting *P. aeruginosa* biofilm development.

Keywords: bacterial cellulose; argon plasma; biofilm; surface modification; immobilization

Citation: Chareza, M.; Ekiert, E.; Moszyński, D.; Madej, M.; Jędrzejczak-Silicka, M.; Drozd, R. An Evaluation of the Usability of Argon Plasma-Treated Bacterial Cellulose as a Carrier for Controlled Releases of Glycoside Hydrolases $PelA_h$ and $PslG_h$, Which Are Able to Eradicate Biofilm. *Appl. Sci.* **2023**, *13*, 7797. https://doi.org/10.3390/app13137797

Academic Editor: Anthony William Coleman

Received: 26 May 2023
Revised: 27 June 2023
Accepted: 28 June 2023
Published: 1 July 2023

1. Introduction

Extensive skin damage is a common health issue that has become a major problem in healthcare systems around the world. Damaged skin loses its natural protective mechanism and becomes a target for microorganisms, leading to severe wound infections, delaying the healing process, disfiguring, and even potentially threatening life [1]. Dynamically developing skin tissue engineering is leading to the development of modern dressing materials. Contrary to standard ones, modern ones are designed not only to cover the surface of the wound but also to support healing; therefore, more advanced materials that are classified as interactive and bioactive are being used [2]. Modern bioactive dressings should be highly hygroscopic to keep the wound bed moist and absorb exudate. In addition, they should ensure a free flow of oxygen and are characterized by a high mechanical

strength and flexibility, thanks to which the dressing can adapt to various parts of the body. It should easily detach from the wound while changing the dressing, be biocompatible, and have homeostatic and antimicrobial action, preventing infection and bacterial biofilm formation [1,3]. One of the biomaterials that meets most of the above criteria is bacterial cellulose (BC) [4]. In addition, the advantage of BC used in biomedicine is also the ability to modify its structure via various in situ and ex situ modifications [5]. The in situ modification of BC can be achieved by supplementing the culture medium with various types of organic and inorganic substances. These modifications can lead to enhanced porosity, water-holding capacity, and rehydration rates, which are crucial properties for wound-dressing materials. However, a significant challenge in the use of biomaterials involving BC is their susceptibility to bacterial infections, which restricts their applications in biomedicine. As a result, there has been a growing interest in the development of methods to confer antibacterial and antibiofilm properties to natural polymeric materials, including bacterial cellulose [6–8].

One of the possible methods for the ex situ modification of BC is the use of plasma, which is a well-known approach for effectively modifying the surfaces of various polymers. Depending on the composition of the gas phase, plasma technology offers the possibility of targeted polymer modification by introducing different functional groups or converting existing ones on the polymer surface. Various gas plasma technologies for polymer modification can be classified into two types based on the temperature of the gas: "hot" plasma and "cold" plasma [9]. Earlier studies have demonstrated that the surface of BC can be improved for various applications through the use of different types of plasmas. The application of nitrogen plasma for BC modification has been found to improve the adhesion of eukaryotic cells to the BC surface and increase its porosity [10,11]. The modification of BC membranes' surfaces using oxygen plasma can lead to a decrease in the effective pore area and water flux, while increasing the number of O-H groups. As a result, there is a significant change in the water contact angle, making the membrane surface more hydrophilic [12]. The modification of BC with argon plasma can confer bactericidal properties, making it suitable for use as antibacterial and antiviral filters based on BC [11]. Moreover, the introduction of new functional groups on the surfaces of polymer matrices through plasma exposure may affect the release process of active compounds, including enzymes, from the surfaces of polymeric materials, especially in applications related to biofilm eradication [13–16].

Pseudomonas aeruginosa and *Staphylococcus aureus* are the most frequently isolated bacterial pathogens found in wounds of various origins. Unlike wounds infected by *S. aureus*, which can readily colonize the upper layers of the wound, *P. aeruginosa* tends to establish itself in the deeper regions of the wound bed, making eradication more challenging. *P. aeruginosa* is known for its high resistance to antimicrobial agents, resulting in a significant prolongation of the wound healing process or even complete stoppage of healing [17,18]. The main reason for the increased risk associated with *P. aeruginosa* infections is its ability to form biofilms, which are recognized as the most significant virulence factors of this bacterium. Biofilms exhibit a complex structure composed primarily of proteins, nucleic acids, lipids, biosurfactants, and exopolysaccharides. The presence of exopolysaccharides plays a crucial role due to their diverse functions, including bacterial adhesion to surfaces, protection against phagocytosis and the immune system, and restriction of antibiotic diffusion within the biofilm structure. *P. aeruginosa* is capable of synthesizing three of the polysaccharides involved in biofilm matrix formation: alginate, Pel, and Psl. However, the specific types and quantities of the polysaccharides produced can vary depending on the strain [19–23]. Psl is a neutral polysaccharide composed of repeating units of D—mannose, D—glucose, and D—rhamnose, while until recently, the exact structure of Pel remained unclear. In the latest research, Le Mauff et al. described the structure of Pel as a linear homopolymer of partially de-N-acetylated α-1,4-GalNAc comprised predominantly of dimeric repeats of galactosamine and N—acetylgalactosamine [24,25]. To prevent the development of these polysaccharide components of the biofilm matrix, it

is possible to use an enzyme with specific activity against the *P. aeruginosa* matrix, such as $PelA_h$ and $PslG_h$ glycoside hydrolases [26–30]. In the field of medicine, it is crucial to develop suitable approaches for creating non-fouling biomaterials. Currently, there is a growing interest in the use of immobilized $PelA_h$ and $PslG_h$ on polymer surfaces in medical applications. These proteins have shown potential in limiting the development of *P. aeruginosa* biofilms, thereby aiding the effectiveness of antibiotics and the immune system. Asker et al. investigated the immobilization of $PslG_h$ on surfaces such as silica glass, polydimethylsiloxane, polystyrene, and indwelling catheters, confirming the ability of surface-attached enzymes to effectively inhibit *P. aeruginosa* biofilm formation. Similarly, Szymanska et al. conducted studies demonstrating that the adsorption of $PelA_h$ on BC surfaces could reduce the polysaccharide components of the *P. aeruginosa* matrix, thereby expanding the utility of BC as a wound-dressing material [26,27,30,31].

The aim of this study was to evaluate the effectiveness of combining surface modification of BC using low-pressure argon plasma (LPArP) with the immobilization of antibiofilm enzymes, namely $PelA_h$ and $PslG_h$, on *P. aeruginosa* biofilm formations.

2. Materials and Methods

2.1. Cloning, Expression, and Purification of $PelA_h$ and $PslG_h$

$PelA_h$ was purified as previously described [26]. To obtain the target gene sequence that encodes the protein construct fragment of *pslG* (GenBank ID AAG05625.1) from the genomic DNA of *P. aeruginosa*, PAO-1 and pET28a were used as a vector template and amplified separately through polymerase chain reactions using Phusion® High-Fidelity DNA Polymerase (New England Biolabs). For *pslG* gene amplification, primers were designed as follows: forward (5′-TGTTTAACTTTAAGAAGGAGATATACCATGGAGATCCAGGTACTGAAGGC-3′) and reverse (5′AGCCGGATCTCAGTGGTGGTGGTGGTGGTGCTCCCAGACCAGCATCTGCA-3′). For pET28a, primers were designed as follows: forward (5′-TGAGATCCGGCTGCTAACAAAGC-3′) and reverse (5′-CATATGGCTGCCGCGCGG-3′). Construct was prepared according to the FastCloning and SLiCE methods [26,32]. The expression and purification of recombinant $PslG_h$ was performed according to previous work [26,32]. To check the purity of the obtained protein, SDS-PAGE analysis was performed. The protein concentration was measured via UV absorbance at 280 nm using a Biotek Synergy HT plate reader (BioTek, Santa Clara, CA, USA) using a molar extinction coefficient equal to 44,920 M^{-1} cm^{-1}, as calculated according to the amino acid sequence of $PelA_h$ (UniProt accession code: Q9HZE4), and 111,840 M^{-1} cm^{-1}, calculated according to the amino acid sequence of $PslG_h$ (UniProt accession code: Q9I1N2).

2.2. Preparation of BC Membranes

The BC production was performed according to Charęza el al., with slight modifications [32]. A culture of *Komagataeibacter xylinus* ATCC® 53524 that was purchased from American Type Culture Collection (ATCC, Manassas, VA, USA) was set up in 9 cm petri dishes with liquid Hestrin–Schramm (HS) medium containing glucose at 20 g/L, yeast extract at 2.0 g/L, peptone at 2 g/L, citric acid at 1.15 g/L, Na_2HPO_4 at 2.7 g/L, and $MgSO_4x7H_2O$ at 0.06 g/L with 1% ethanol and 0.01% of silicone polyether. Before pouring the cultivation medium on the petri dishes, the medium was inoculated with 1% of a 1-week-old culture of *K. xylinus* that was previously shaken vigorously for 5 min. The cultivation was carried out at 28 °C for 4 days. After this time, the formed BC membranes were collected and transferred to plastic containers with deionized water for 24 h at 4 °C. In the next step, the BC membranes were digested with 0.1 M of NaOH at 80 °C (3×) to remove bacterial cells and residual medium components. Following digestion, the BC membranes were transferred again to plastic containers with extensive amounts of deionized water. The water was changed periodically until the pH stabilized to a neutral range. Finally, the pure BC membranes were dried at 64 °C and sterilized by autoclaving at 121 °C for 15 min.

2.3. Modification of BC with Low-Pressure Argon Plasma (LPArP)

LPArP treatment of the BC membranes was performed using an HPT-100 Benchtop Plasma Treater (Henniker Scientific, Runcorn, UK). The process was carried out with argon as the process gas in the gas chamber, at a power of 100 W and flow rate of 10 standard cubic centimeters per minute (SCCM) that was constant in all experiments. To determine the optimal time for BC modification, the samples were treated with LPArP for various durations of 120, 240, 480, and 960 s from both sides.

2.4. Characterization of BC Surfaces after LPArP Treatment

2.4.1. Attenuated Total Reflectance–Fourier Transform Infrared Spectroscopy (ATR–FTIR)

After the Ar plasma modification of the BC, the chemical structure of the surfaces of BC was analyzed using ATR-FTIR. The analysis was carried out using an ALPHA II FTIR spectrophotometer (Bruker Daltonic, Bremen Germany) with a diamond ATR adapter. The spectra were collected in the wavenumber range of 3800–400 cm^{-1} with a resolution of 2 cm^{-1} (32 scans). The processing of collected ATR-FTIR spectra was performed using SpectraGryph 1.2 and OriginPro2021 software. The IR indices of the BC crystallinity, such as the total crystallinity index (TCI), lateral order index (LOI), and hydrogen bond intensity (HBI), were calculated from the band's absorbance ratios of A1371 cm^{-1}/A2900 cm^{-1}, A1429 cm^{-1}/A897 cm^{-1}, and A3400 cm^{-1}/A1320 cm^{-1}, respectively. The allomorph I_α content was calculated using Equation (1):

$$I_\alpha \alpha = 2.55 - \left(\frac{\text{A750}}{(\text{A710} + \text{A750})} \right) - 0.32 \quad (1)$$

where A750 is a band intensity of 750 cm^{-1} for I_α, and A710 is a band intensity of 710 cm^{-1} for I_β.

2.4.2. X-ray Photoelectron Spectroscopy (XPS)

X-ray photoelectron spectra were obtained using Mg Ka (hν = 1253.6 eV) radiation with a Prevac system equipped with a Scienta SES 2002 electron energy analyzer operating at a constant transmission energy (Ep = 50 eV). The samples were attached to a stainless steel holder with the use of carbon conductive double-sided adhesive discs. Charging effects were corrected by assuming that the maximum of the C 1s peak corresponded to the aliphatic carbon bindings of C-OH in cellulose, and its location was set to 286.7 eV [33]. The XPS lines of the other observed elements were shifted correspondingly. The reproducibility of the peak positions thus obtained was ±0.1 eV. The surface compositions of the samples were obtained on the basis of the peak area intensities using the sensitivity factor approach and assuming homogeneous composition of the surface layers.

2.4.3. Scanning Electron Microscopy (SEM)

Prior to SEM analysis, samples of BC membranes, both LPArP-modified and nonmodified, were immersed in 2% glutaraldehyde for 16 h. Then the samples were flushed with 50 mM of phosphate buffer at pH 7.4. Following, BC samples were immersed in increasing concentrations of ethanol (20%, 40%, 60%, 80%, 95% v/v) for 10 min and finally immersed two times in absolute ethanol for 15 min. Then samples were sputtered with Cr using a SEM Quorum Q150T ES, a turbomolecular-pumped coater, and analyzed with using a Hitachi SU3500 (Hitachi, Tokyo, Japan) scanning electron microscope [7,34].

2.5. $PelA_h$ and $PslG_h$ Stability—Differential Scanning Fluorimetry (DSF)

Differential scanning fluorimetry employing the Prometheus NT.48 apparatus (NanoTemper Technologies GmbH, München, Germany) was used to investigate the thermal stability of $PelA_h$ and $PslG_h$ at given time points during storage at 4 °C as protein solutions or lyophilisates. The lyophilisates of $PelA_h$ and $PslG_h$ were resuspended in distilled water at concentrations of 0.3 mg/mL. The $PelA_h$ and $PslG_h$ in the solutions were used at con-

centrations of 0.3 mg/mL. The samples were then loaded into nanoDSF standard-grade capillaries and then heated from 20 °C to 95 °C at a rate of 1 °C per min. Protein unfolding was monitored by measuring the fluorescence intensity at two emission wavelengths of 330 nm and 350 nm. Analysis of the obtained data was performed using PRThermControl software (NanoTemper Technologies GmbH, München, Germany), which allowed calculation of the proteins' melting temperatures (T_m) based on the first derivative of the ratio of fluorescence intensity measured at 350 and 330 nm. Four independent measurements of T_m were performed for each time point.

2.6. Analysis of the Cytotoxicity of $PslG_h$ Hydrolase

The potential cytotoxicity of the recombinant enzyme was analyzed using an L929 mouse fibroblast (ATCC® no. CCL-1™). In vitro dose–response experiments were conducted using the CCK-8 Cell Counting Kit-8 (Sigma-Aldrich, St. Louis, MO, USA). Firstly, cells (passages 20–25) were maintained in standard cell culture conditions at 37 °C, 5% CO_2, and 95% humidity in T25 flasks (Sarstedt, Nümbrecht, Germany) in complete DMEM culture medium that was supplemented with 10% heat-inactivated fetal bovine serum (FBS) (PAA Laboratories GmbH, Pasching, Austria), 2 mM L-glutamine, 50 IU/mL penicillin, and 50 µg/mL streptomycin (Corning Inc., Corning, NY, USA). For the CCK-8 assay, cells were plated into the wells of 96-well plates (at 5×10^3 cells per well for a 24 h observation and 10×10^3 cells per well for a 48 h observation). Secondly, twenty-four hours after cell seeding, 6 different final concentrations (5.0, 10.0, 25.0, 50.0, 100.0, 250.0 µg/mL; 5 replicates of each dose) of the enzyme were prepared in DMEM medium and added to the cells. The effect of the recombinant enzyme on cell viability was calculated using Equation (2), as described elsewhere [35]:

$$\text{Relative viability from CCK-8 assay } (\%) = \left(\frac{\text{sample } A_{450–650 \text{ nm}}}{\text{control } A_{450–650 \text{ nm}}} \right) \times 100 \quad (2)$$

where A is an absorbance at 450 nm and 650 nm.

The morphologies of the L929 cell line exposed to the recombinant enzyme at different concentrations and the control samples were analyzed using a Nikon TS-100 phase-contrast inverted microscope (NIS Elements F Package, camera Nikon DS-Fi1, Nikon, Melville, NY, USA) at 100× magnification [35].

2.7. The Loading of $PelA_h$ and $PslG_h$ on BC and Ar_BC

The solutions of $PelA_h$ and $PslG_h$ proteins (0.5, 0.25, and 1.25 and mg/mL) were prepared in 50 mM phosphate buffer at pH 7.4, which corresponded to 2.5, 1.25, and 0.62 µg of protein in 5 µL. The 5 µL of protein was loaded onto Ar treatment and non-treatment BC samples with a diameter of around 6 mm. Next, the samples with loaded protein were frozen using dry ice until the samples were completely frozen. Finally, the samples were freeze dried (Alpha 1–2 LDplus, Christ, Germany) at −60 °C and 0.1 mBar.

2.8. Analysis of In Vitro Release of $PelA_h$ and $PslG_h$ from Ar_BC and BC

The samples of immobilized proteins on LPArP-modified and pristine BC were transferred to Eppendorf tubes with 500 µL of 50 mM phosphate buffer, pH 7.4, and equilibrated to 25 °C in thermoblock. Next, in one-minute intervals, 2 µL of solution was transferred to a Take3 microvolume plate for the determination of the proteins' concentrations according to protocol described in Section 2.1.

2.9. Antibiofilm Activity

The antibiofilm activity of BC membranes with immobilized $PelA_h$ and $PslG_h$ was conducted according to Amborgi et al., with modifications [36]. The strain of *P. aeruginosa* PAO-1 was grown in TSB medium supplemented overnight at 37 °C. For biofilm analysis, the overnight culture of *P. aeruginosa* PAO-1 was adjusted to 0.5 on the McFarland scale and then diluted to 1:1000 in TSB medium supplemented with 1% glucose. A total of 100 µL

of bacterial suspension was transferred to 96-well flat plates and incubated at 37 °C for 24 h with the presence or in absence of LPArP-modified BC membranes or nonmodified BC. After incubation, the biofilm as washed with 200 µL of distilled water and then dried at 37 °C for 1 h. Next, 100 µL of 0.1% crystal violet was added to each well and incubated for 15 min. Following incubation, the wells were washed with 200 µL of dH_2O until unbound dye was removed. Finally, 100 µL of 96% ethanol was added to each well, incubated for 15 min, and the absorbance of crystal violet was measured at 595 nm using a Tecan Infinite 200 Pro microplate reader.

2.10. Statistical Analysis

Statistical analysis was conducted using OriginPro2021. The statistical significance differences of means were tested by Tukey's multiple comparison test, and statistical significance was considered with $p < 0.05$.

3. Results and Discussion

3.1. Influence of LPArP Treatment on BC Membrane Surface Properties

To analyze the changes in the chemical structure of the BC surfaces after treatment with LPArP, the ATR-FTIR and XPS methods were used. Figure 1 presents the regions of 1800–800 cm^{-1} of the ATR—FTIR spectra of the untreated BC and the BC treated with LPArP, depending on the treatment time. The obtained spectra from all tested BC samples showed the characteristic absorption band profile for BC, with bands at 897 cm^{-1} assigned to C-O-C bending vibration of (1–4) β linkage, ~1060–1030 cm^{-1} corresponding to C-O stretching, 1111 cm^{-1} assigned to the C-C stretching ring in polysaccharides, ~1160 cm^{-1} indicating C-O-C stretching of the glycosylic bond of the crystalline cellulose, 1370 cm^{-1} assigned to C-H stretching vibrations, and 1430 cm^{-1} indicating the symmetric CH_2 bending vibration and referred to as a "crystallinity band". The next band at 1640 cm^{-1} marks the H-O-H bending of absorbed water molecules [37–41]. The time-dependent BC surface treatment with LPArP was evident in the spectra through a gradual increase in the intensity of absorption in the band at 1720 cm^{-1}, which is attributed to the carbonyl group (C=O stretching vibrations) [42]. The intensity of this band increased with time and reached a plateau after 480 s of treatment with the LPArP. The appearance of this band can indicate the oxidation of the -OH group of anhydrous D-glucose units in the BC microfibrils or the formation of a carbonyl group after pyranose ring cleavage between C1 and C2 and further oxidation [43]. It is also in accordance with the observed reduction in band intensity at a wavelength range of ≈1050 cm^{-1}—≈950 cm^{-1} that can be associated with conformational changes in the pyranose ring and the primary alcohols at the C6 carbon typical for more amorphous bacterial cellulose.

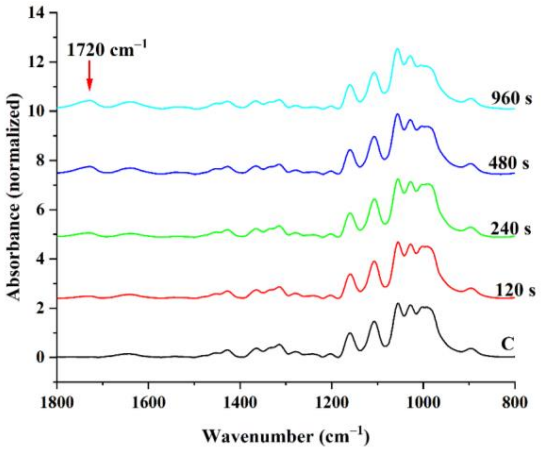

Figure 1. The ATR—FTIR spectra of the control BC (C) and the BC modified with LPArP for various times (120 s, 240 s, 480 s, and 960 s). The red arrow marking the changes in the intensity of the band at 1720 cm^{-1} is assigned to the C=O group. The spectra were normalized to band area at 1161 cm^{-1}.

The values of the IR crystallinity indices LOI and TCI decreased with the modification time, while the value of the HBI increased (Table 1). The most significant changes in the IR crystallinity indices were noted until 480 s of treatment. The changes in values of TCI and LOI clearly indicated that the structure of LPArP-treated BC is characterized by lower crystallinity and ordered structure as a result of the destructive action of the argon plasma [38,44].

Table 1. The values of the IR crystallinity indices (LOI, TCI), the hydrogen bond index (HBI), and the mass fraction of the crystalline allomorph I_α of pristine BC and BC modified by LPArP.

Sample	IR Crystallinity		HBI	Cellulose I_α Index
	A1372/A2900 (TCI)	A1429/A897 (LOI)	A3400/A1320	
BC	1.683 ± 0.20 ^{a}	0.993 ± 0.17 ^{a}	0.801 ± 0.08 ^{a}	0.683 ± 0.02 ^{a}
120 s Ar_BC	1.685 ± 0.04 ^{a}	0.877 ± 0.10 ^{ab}	0.751 ± 0.03 ^{a}	0.667 ± 0.01 ^{ab}
240 s Ar_BC	1.673 ± 0.08 ^{a}	0.849 ± 0.04 ^{ab}	0.899 ± 0.10 ^{a}	0.650 ± 0.02 ^{bc}
480 s Ar_BC	1.492 ± 0.10 ^{b}	0.818 ± 0.09 ^{b}	1.266 ± 0.15 ^{b}	0.637 ± 0.02 ^{c}
960 s Ar_BC	1.351 ± 0.07 ^{b}	0.766 ± 0.04 ^{b}	1.468 ± 0.16 ^{c}	0.611 ± 0.006 ^{d}

The results are presented as means ± S.D. The means with the same superscript are not significantly different, with $p > 0.05$.

3.2. X-ray Photoelectron Spectroscopy (XPS)

X-ray photoelectron spectroscopy was applied to evaluate the surface composition of the LPArP-treated BC. Analysis of the XPS spectra indicated only the presence of oxygen and carbon on the surfaces of the samples. The ratio of oxygen atoms to carbon atoms on the surfaces of the studied materials was determined from the atomic concentration of these elements, which was calculated from the intensity of the XPS signals: O 1s and C 1s (Table 2). The calculations assumed a homogeneous distribution of oxygen and carbon atoms in the surface layer. Considering the formula of cellulose as $(C_6H_{10}O_5)_n$, the theoretical ratio of oxygen atoms to carbon atoms in this material is 0.83. According to the study of the surface composition, it was lower than the theoretical value for all tested materials and ranged from 0.56 to 0.73, with the lowest value of the O/C ratio observed for the sample obtained after 480 s of plasma exposure. The highest O/C ratio was observed not for a pure cellulose sample, but for a sample exposed to plasma for only 120 s. Such relative enrichment of the surface with oxygen atoms can be attributed to the partial etching of the cellulose surface from "adventitious carbon" caused by argon ions.

Table 2. The percentage of Comp (**1**)–Comp (**4**) components in the total signal of the XPC C 1s line and the ratio of oxygen atoms to carbon atoms on the surfaces of bacterial cellulose exposed to LPArP depending on the treatment time (s).

Sample	Components of XPS C 1s Signal (Total C1 s Intensity = 100)				
	C-C/C-H (Comp (1))	C-OH (Comp (2))	COC (Comp (3))	O=C-O (Comp (4))	O/C Ratio
BC	14	61	25	0	0.69
120 s Ar_BC	19	53	20	7	0.73
240 s Ar_BC	26	49	17	7	0.62
480 s Ar_BC	34	39	18	8	0.56
960 s Ar_BC	38	33	21	6	0.64

The high-resolution spectra of the XPS C 1s lines acquired for all examined samples are presented Figure 2. A deconvolution model which consists of four basic components of C 1s transition was applied. The component denoted as Comp (**1**), having a binding energy of 285.0 ± 0.1 eV, essentially corresponds to nonfunctionalized carbon atoms. The component Comp (**2**), having a binding energy of 286.7 eV, is ascribed to a group of differently bonded

carbon atoms linked to one atom of oxygen, as in hydroxyl group C-OH. Comp (**3**), located at a binding energy of 288.2 ± 0.1 eV, is ascribed to O-C-O bonding. The component Comp (**4**), having a binding energy of 289.6 ± 0.1 eV, corresponds to O-C=O bonding. The values of the binding energies used in the present model are based on the deconvolution models applied elsewhere [33]. The percentage of Comp (**1**)–Comp (**4**) components in the total signal of the XPS C 1s line is presented in Table 2.

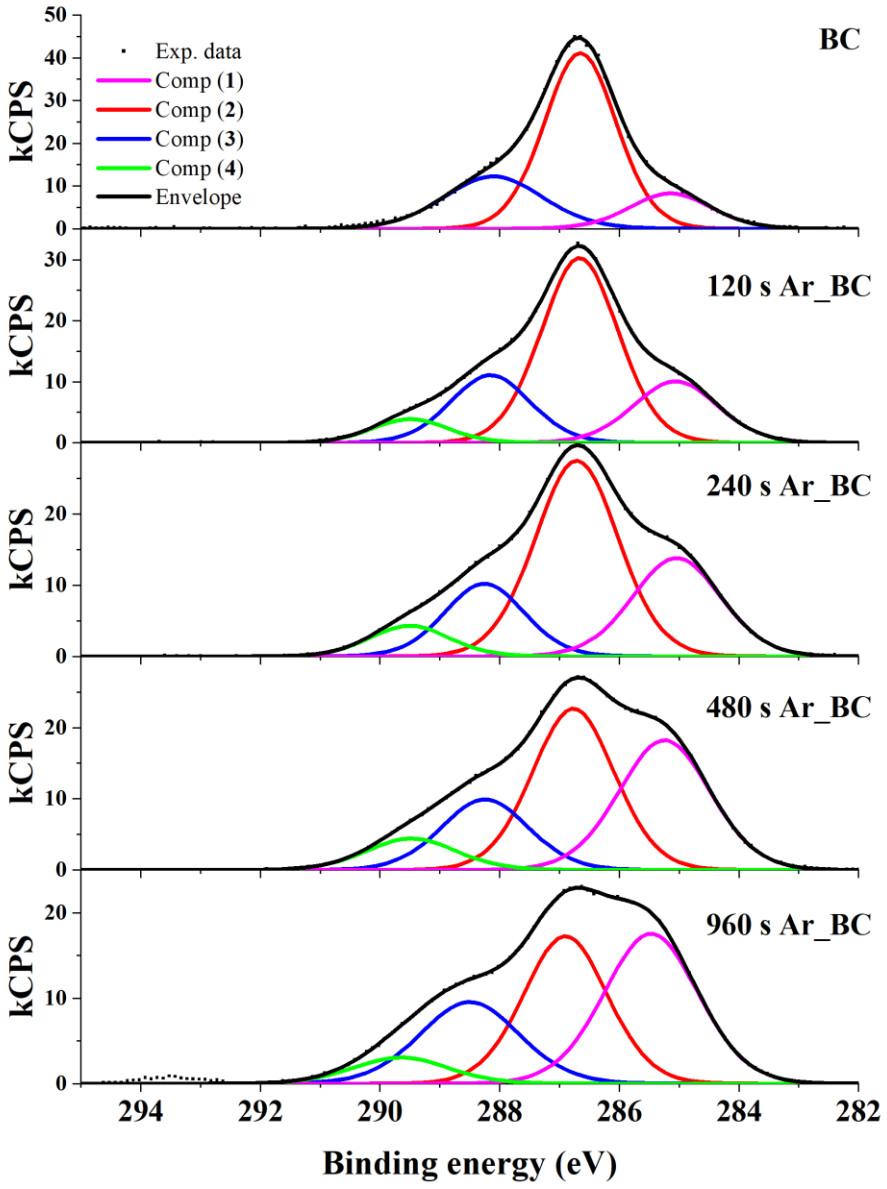

Figure 2. High-resolution XPS C 1s spectra of non-modified BC and bacterial cellulose (Ar_BC) modified by different exposure times to LPArP.

Highly purified bacterial cellulose should contain only carbon–oxygen bonds corresponding to Comp (**2**) and Comp (**3**) of the model used to analyze the XPS C 1s spectra. The theoretical ratio of these components should be 80:20, respectively. It is common for real cellulose samples to have Comp (**2**) accounting for about 60% of the signal from carbon atoms and Comp (**3**) about 20% of this signal. In actual samples, even of pure cellulose, a component corresponding to Comp (**1**) is also identified, which accounts for less than 20% of the C 1s signal [43]. The XPS C 1s spectrum of the reference material (BC) used in this study was very close to those reported. Exposure of this material to plasma results in several characteristic changes in the composition of its surface. As the exposure to

plasma increases, the concentration of Comp (**2**) decreases and the concentration of Comp (**1**) unequivocally increases. The decrease in Comp (**2**) is most likely due to the removal of hydroxyl groups from the cellulose surface. The removal of such bonds is accompanied by a simultaneous increase in the concentration of C-C- or C-H-type bonds, i.e., Comp (**1**). The concentration of Comp (**3**) is essentially independent of the plasma exposure. This component corresponds to the presence of an O-C-O bond at the C_1 carbon in the pyranose ring. This suggests the stability of the pyranose ring during the plasma action on the cellulose surface. The exposure to argon plasma also induces the appearance of Comp (**4**), which is directed to the oxidation of D-glucose alcoholic group C-OH without significant effect on the integrity of the pyranose ring. The changes in the BC surface composition demonstrated by the XPS analysis are in good agreement with the ATR-FTIR and showed that BC surfaces can be more negatively charged as a result of the presence of the carboxyl group.

3.3. Influence of LPArP on the BC Surface Morphology

In order to check the morphological changes in the BC structure after LPArP modification, scanning electron microscopy was used. Figure 3 shows the SEM micrograph of BC surface morphology (a) and the Ar_BC after modification with LPArP for 480 s (b). The unmodified BC sample shows a typical reticulated surface of pristine BC with a well-visible ultra-fine network of microfibrils and pores [45,46]. After modification with LPArP, the surface morphology of the BC changed significantly and presented a heterogeneous structure typical for amorphous BC. These results are consistent with the studies by Tang et al. and Vasil'kov et al., where they reported that the oxygen plasma treatment of BC can cause a burn of the surface which results in an increase in the surface roughness and heterogeneity due to the destruction of the BC fibril structure [47,48].

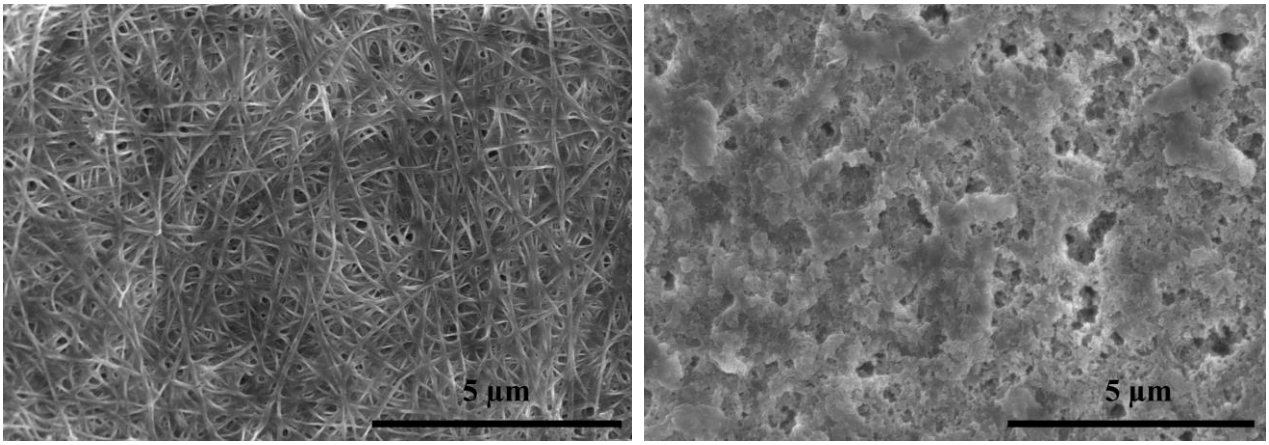

(**a**) (**b**)

Figure 3. SEM images of the surface morphology the BC (**a**) and Ar_BC after 480 s LPArP treatment (**b**).

3.4. Differential Scanning Fluorimetry

In recent years, the importance of protein preparations in medicine has increased significantly; however, most of the preparations available on the market are in liquid form, which requires storage at low temperatures. This is associated with difficulties with high transport costs, among others. Moreover, during long-term storage of proteins in solutions, the activity of proteases shortens their activity time and also causes reactions such as oxidation, leading to protein unfolding that may also occur [49,50]. One method to overcome these obstacles is to store proteins in lyophilized form. In order to determine the usefulness of the $PelA_h$ and $PslG_h$ enzymes in freeze-dried and soluble form, their stability was tested after 30 days using the DSF method, which is a biophysical technique widely used to study the thermal stability of a protein [51]. Figure 4 shows the plot of the

first derivative of the fluorescence melting curves of $PelA_h$ and $PslG_h$ in freeze-dried and soluble form at the beginning and after 30 days of storage at 4 °C. The T_m values of the $PelA_h$ in the soluble form were 52.7 °C and 52.8 °C at days 0 and 30 of storage, respectively, while upshifting of the freeze-dried form by ~1.3 °C was observed after 30 days, suggesting the acquisition of a slight thermal structural stability. In the case of the soluble form of $PslG_h$, there was no significant difference in the T_m value during the storage conditions (T_m equal to ~53.1 °C), and the same observations were made with the freeze-dried form (T_m equal to ~53.7 °C).

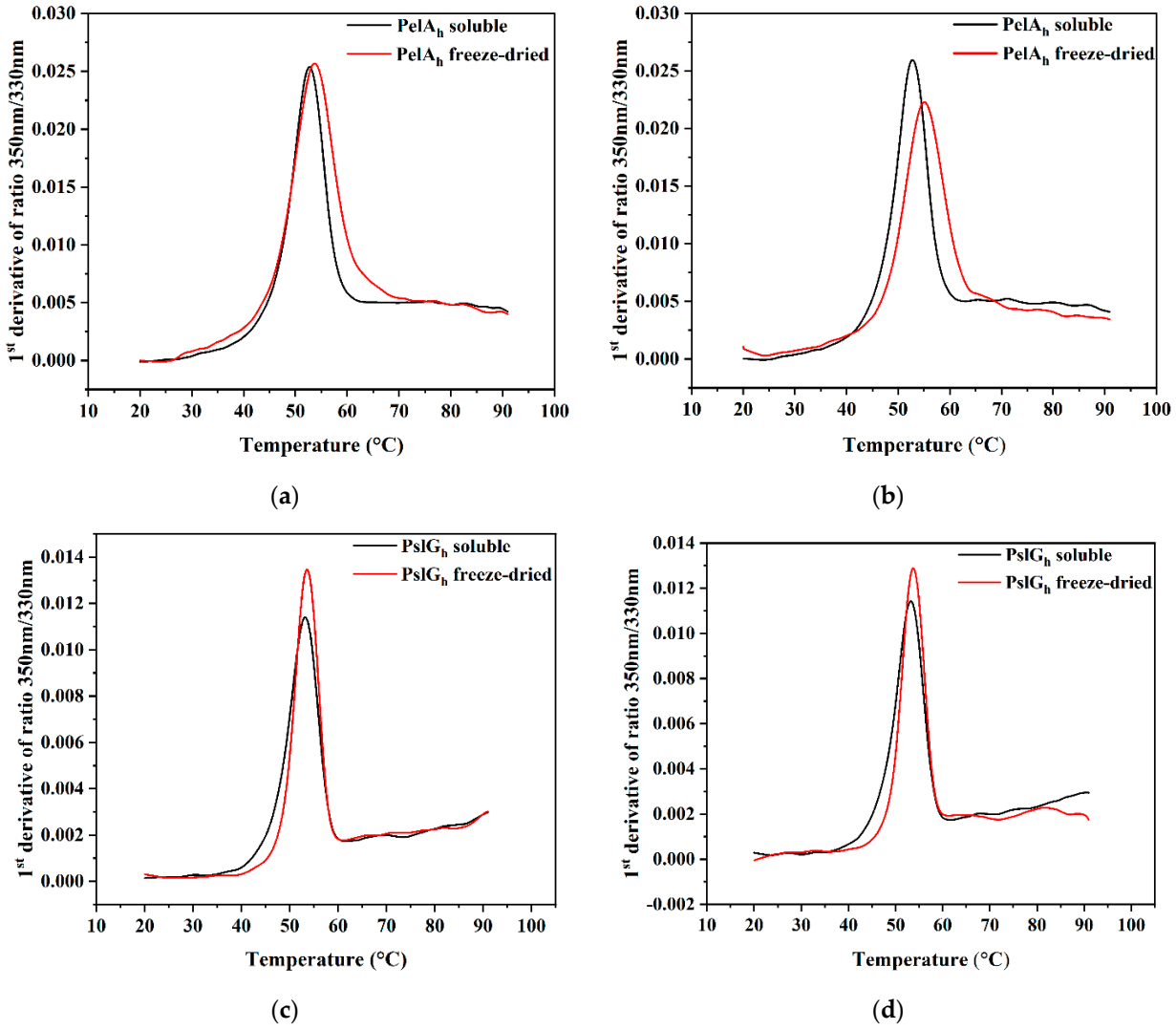

Figure 4. The thermal stability profile of soluble and freeze-dried forms of $PelA_h$ and $PslG_h$ stored at 4 °C on day 0 (**a**,**c**) and after 30 days of storage (**b**,**d**).

3.5. Cytotoxicity of the $PslG_h$

To enable the use of recombinant enzymes in biomedicine, among other things, as elements of wound-dressing materials, it is important to assess their cytotoxicity against eukaryotic cells. The cytotoxicity of $PelA_h$ was investigated in our previous research, and we concluded that there is no cytotoxicity effect of the enzyme on murine fibroblast (L929) cultures [26].Therefore, the $PslG_h$ enzyme obtained in this study was also tested to determine its potential cytotoxicity towards murine fibroblast (L929) cultures. Six different enzyme concentrations (5.0, 10.0, 25.0, 50.0, 100.0, and 250.0 µg/mL) were used for 24 h and 48 h observations of cell viability and morphology. After 24 h, no reduction in cell viability (Figure 5a) and cell morphology (Figure 6) was observed. After 48 h, the cell morphology

for the experimental cultures did not demonstrate changes in comparison to the control culture. In the case of cell viability, a ~29% reduction was found for the 250.0 µg/mL enzyme concentration (Figure 5b). These results are consistent with earlier studies on the cytotoxicity of $PelA_h$ and $PslG_h$ against eukaryotic cells from line IMR-90 of human lung fibroblasts and red blood cells [27,28].

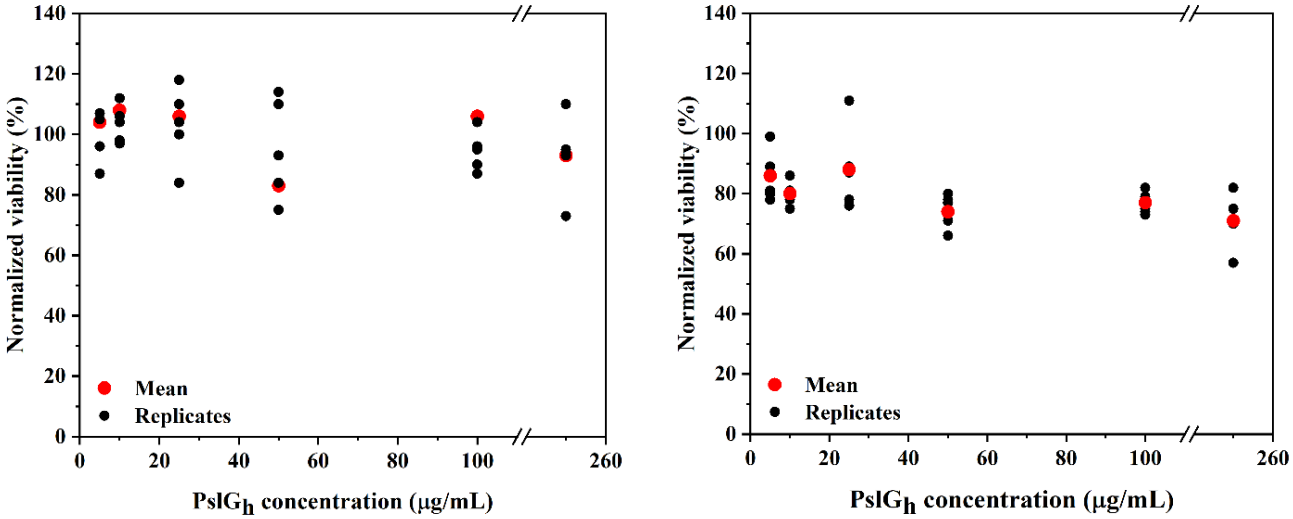

Figure 5. L929 cell viability after 24 h (**a**) and 48 h (**b**) incubation with the recombinant $PslG_h$.

3.6. In Vitro Release Study of $PelA_h$ and $PslG_h$ from Pristine and LPArP-Modified BC

The immobilization of proteins on different kinds of surfaces is used in many areas of industry, including the biomedical and pharmaceutical industries in drug delivery systems [49]. To evaluate the $PelA_h$ and $PslG_h$ from the BC and LPArP-modified BC, the release behavior was monitored in 50 mM of phosphate buffer at pH 7.4. The release profiles of $PelA_h$ and $PslG_h$ are shown in Figure 8. The release profiles of $PelA_h$ from the BC and Ar_BC membranes did not differ and were characterized by sustained diffusion. The same release profile was observed for the $PslG_h$ from nonmodified BC, while the $PslG_h$ released from Ar_BC was characterized by an initial burst release for 2 min. In both cases, higher amounts of enzyme were retained on the BC matrix, and the maximum releases of $PslG_h$ were 58% and 63% after 10 min for BC and Ar_BC, respectively. For $PelA_h$, the % of release from the carrier was faster compared to $PslG_h$, and the maximum release at the same time was around 80% for both unmodified and modified BC. The observed $PelA_h$ release profile did not differ between the unmodified and LPArP-modified BC, but it showed a significantly faster release of this protein compared to $PslG_h$. The charge distributions on the molecular surfaces of the analyzed enzymes at pH 7.4 showed the occurrence of large negatively charged patches. The calculated charges of the protein molecules did not differ significantly between $PelA_h$ and $PslG_h$ and were −8.24 and −6.94, respectively (Figure 7). In contrast to $PelA_h$ the structure of $PslG_h$ consist of large catalytic N- terminal domain and significantly smaller C-terminal domain recognized as possible carbohydrate binding domain (Figure 7). Occurrence of this domain in PslG structure was reported as reason of higher binding to dextran and may be reason of different releasing profile. Furthermore, the differences in release profile of $PslG_h$ from native and LPArP-modified BC suggest that the CBM occur in $PslG_h$ molecular structure belongs to Type B CBMs, which has affinity to amorphous form of BC.

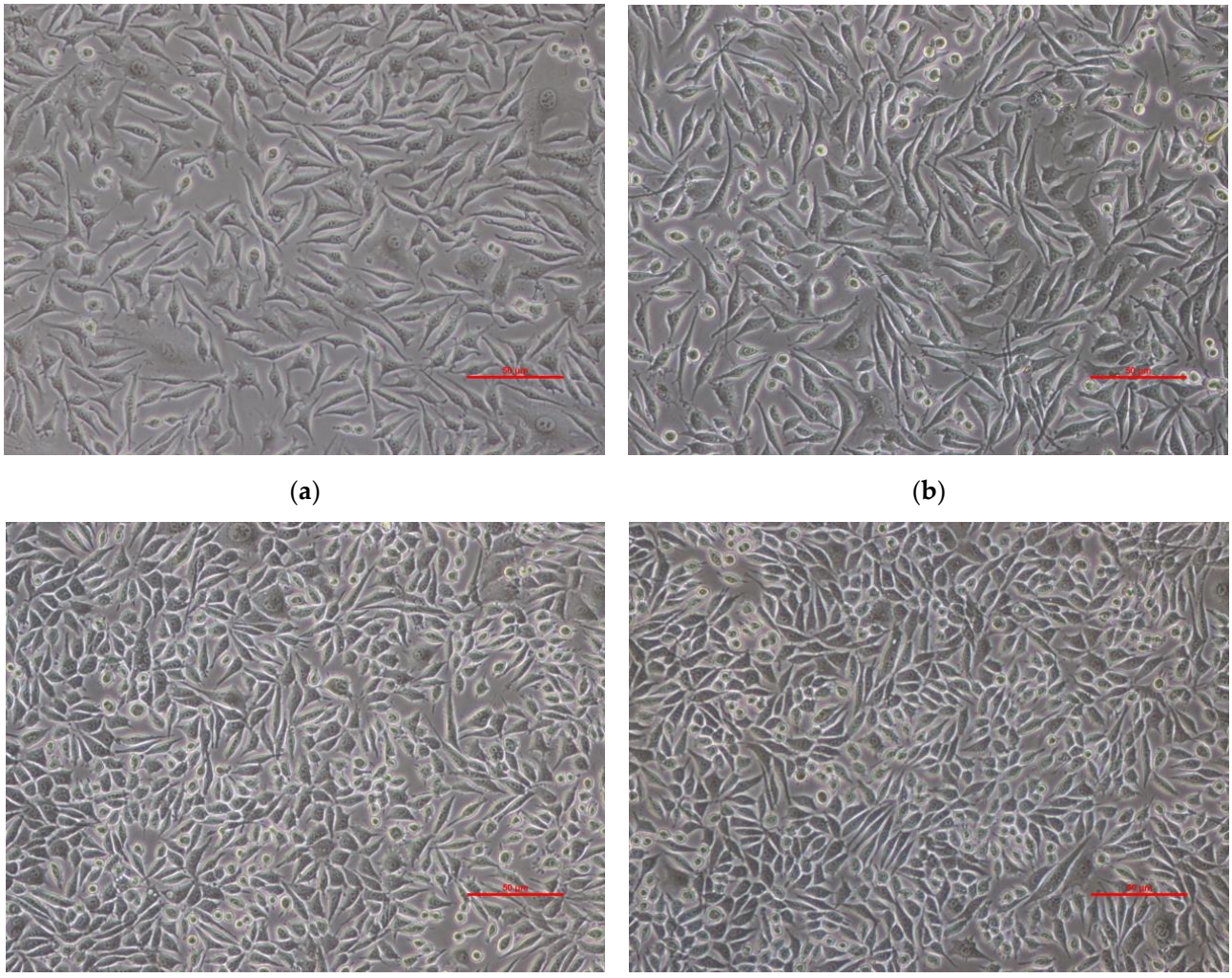

Figure 6. Morphology of L929 cells of 24 h (**a**) and 48 h controls (**c**) and exposed to the recombinant $PslG_h$ (250 µg/mL) for 24 h (**b**) and 48 h (**d**).

To explain the enzymes' release mechanisms from the BC and Ar_BC, pharmacokinetic models were used, including zero-order, first-order, Higuchi, and Korsmeyer-Peppas models. The fitting results are summarized in Table 3. For the $PslG_h$ loaded on the nonmodified BC, the release of the protein was fitted to the Higuchi and Korsmeyer-Peppas models for both types of BC, which indicated that the release of $PslG_h$ is controlled by diffusion. The n exponents of the Korsmayer-Peppas model were around 0.25 and 0.22 for the LPArP-modified and native BC, respectively. This demonstrated that $PslG_h$ was released through Fickan diffusion. In the case of $PelA_h$, it was observed that the release profile for the Ar_BC fit well with the first order, with a correlation coefficient of R^2 equal to 0.98, which indicates that the $PelA_h$ release is dependent on the differential concentration [54]. Moreover, the $PelA_h$ release mechanism also fit the Higuchi and Korsmayer-Peppas models, with a correlation coefficient of $R^2 > 0.9$. The value of exponent n for the $PelA_h$ release was >0.5 and followed non-Fickan diffusion [54,55].

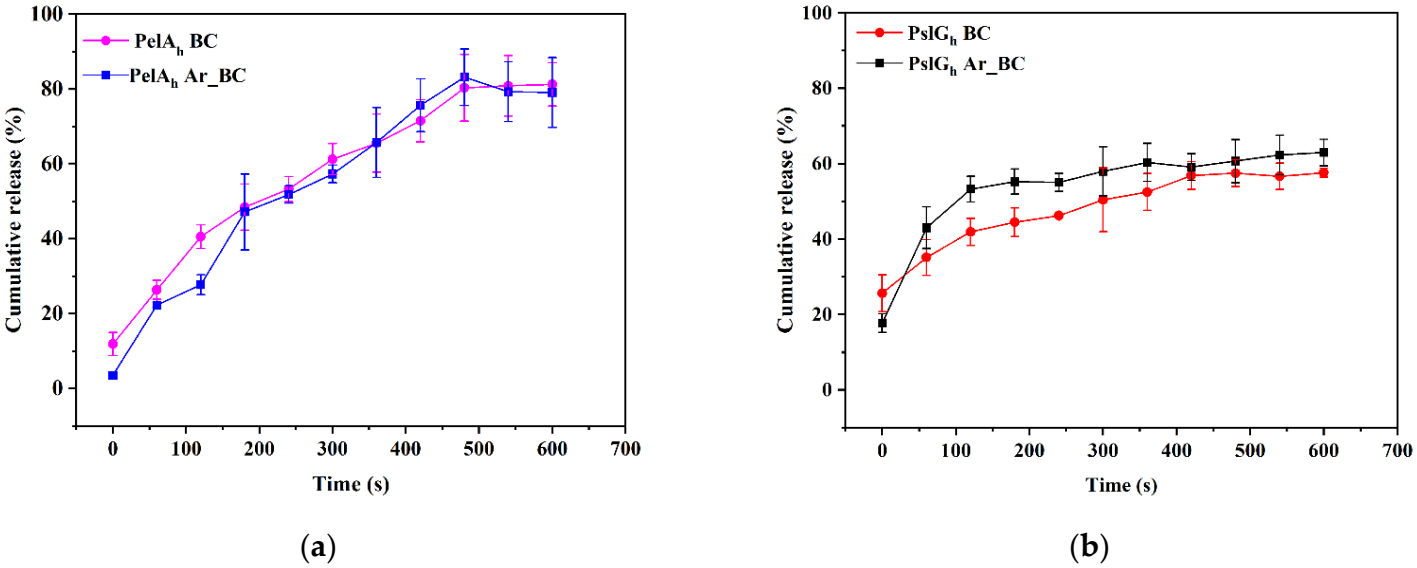

(**a**) (**b**)

Figure 7. The 3D crystal structure models of PelA$_h$ (PDB:5TCB) and PslG$_h$ (PDB:5BX9) proteins with highlighted elements of secondary structure and distribution of the electrostatic potential of their molecular surfaces. The electrostatic potential of the protein molecules' molecular surfaces at pH 7.4 was computed according to predictions of the pKa value by the PROPKA server and the APBS solver via the PDB2PQR server. The final analysis was performed with UCSF Chimera 1.17.1rc package [52,53].

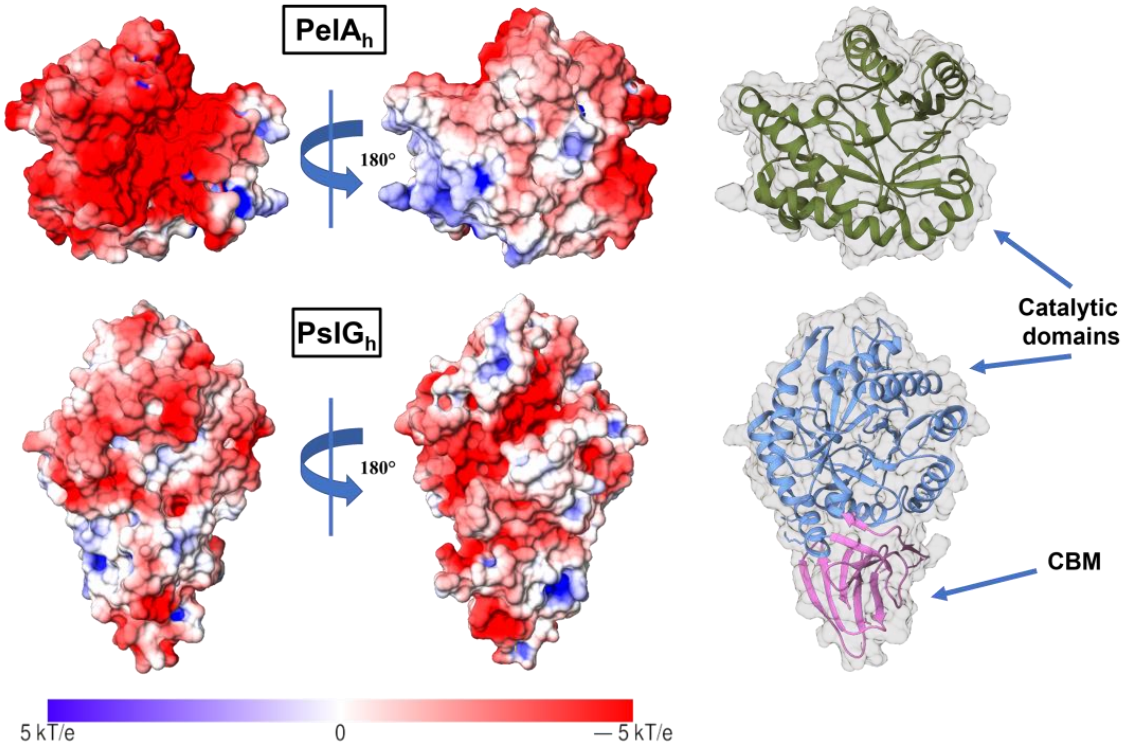

Figure 8. Experimental in vitro PelA$_h$ (**a**) and PslG$_h$ (**b**) release profiles from BC and Ar_BC (in 50 mM phosphate buffer at pH 7.4.

Table 3. Release constants and correlation coefficients of the model equation applied to $PelA_h$ and $PslG_h$ release from native BC and LPArP-modified BC.

Sample	Mathematical Model								
	Zero-Order		First-Order		Higuchi		Korsmeyer-Peppas		
	K_0	R_0^2	K_1	R_1^2	K_H	R_H^2	K_{K-P}	R_{K-P}^2	n
$PelA_h$—Ar_BC	1.24×10^{-3}	0.92	-2.7×10^{-3}	0.98	0.034	0.97	0.016	0.93	0.63
$PelA_h$—BC	1.13×10^{-3}	0.94	-2.7×10^{-3}	0.98	0.031	0.98	0.033	0.98	0.51
$PslG_h$—Ar_BC	5.1×10^{-4}	0.60	-9.8×10^{-4}	0.71	0.016	0.85	0.15	0.90	0.25
$PslG_h$—BC	4.9×10^{-4}	0.88	-9.1×10^{-4}	0.92	0.014	0.98	0.14	0.98	0.22

3.7. Influence of the Immobilization of $PelA_h$ and $PslG_h$ on P. aeruginosa PAO-1 Biofilm Eradication

The effect of $PelA_h$ and $PslG_h$ in soluble and immobilized forms on the ability of *P. aeruginosa* PAO-1 to form biofilm was measured in a microplate model using crystal violet staining. The results for the biofilm inhibition assay are presented in Figure 9. For the soluble form of $PslG_h$, around 70% of the biofilm inhibition was observed when 2.5 and 1.25 µg of enzyme were applied, while for 0.62 µg, the inhibition was slightly lower, amounting to around 50% (Figure 9a). When $PelA_h$ in the same concentration was added to the culture medium, the biofilm inhibition rate was lower compared to $PslG_h$ and was around 50% for 2.5 and 1.25 µg of enzyme and 30% for 0.62 µg (Figure 9d). The composition of the *P. aeruginosa* biofilm matrix is strain dependent. The tested strain of *P. aeruginosa* PAO-1 produces mainly Psl as a dominant exopolysaccharide of the biofilm matrix, which may be the reason for the more effective inhibition of biofilm formation after the use of the $PslG_h$ enzyme [56,57]. In the case of the immobilized enzymes on native BC, it was observed that the biofilm inhibition rate was slightly lower compared to the soluble forms of $PelA_h$ and $PslG_h$ due to lowering release rate of the proteins into the culture medium (Figure 9b,e). The biofilm inhibition rate for the $PelA_h$ released from the Ar_BC (Figure 9f) was similar to the native enzyme released from the BC. The $PslG_h$ released from the Ar_BC exhibited significantly higher inhibiting activity against biofilm development compared to the enzyme released from the unmodified BC, which is consistent with the obtained protein release results. As shown in Figure 9b, for 2.5 µg and 1.25 µg of $PslG_h$ loaded on Ar_BC, the biofilm inhibition rates were 63% and 55%, whereas for protein released from the nonmodified BC, the biofilm inhibition rates were 57% and 53%, respectively. The highest influence of BC modification by LPArP was observed for the concentration of $PslG_h$ equal to 0.62 µg, whereas for nonmodified CB, the biofilm inhibition rate was 12%, while for Ar_BC it was 43%.

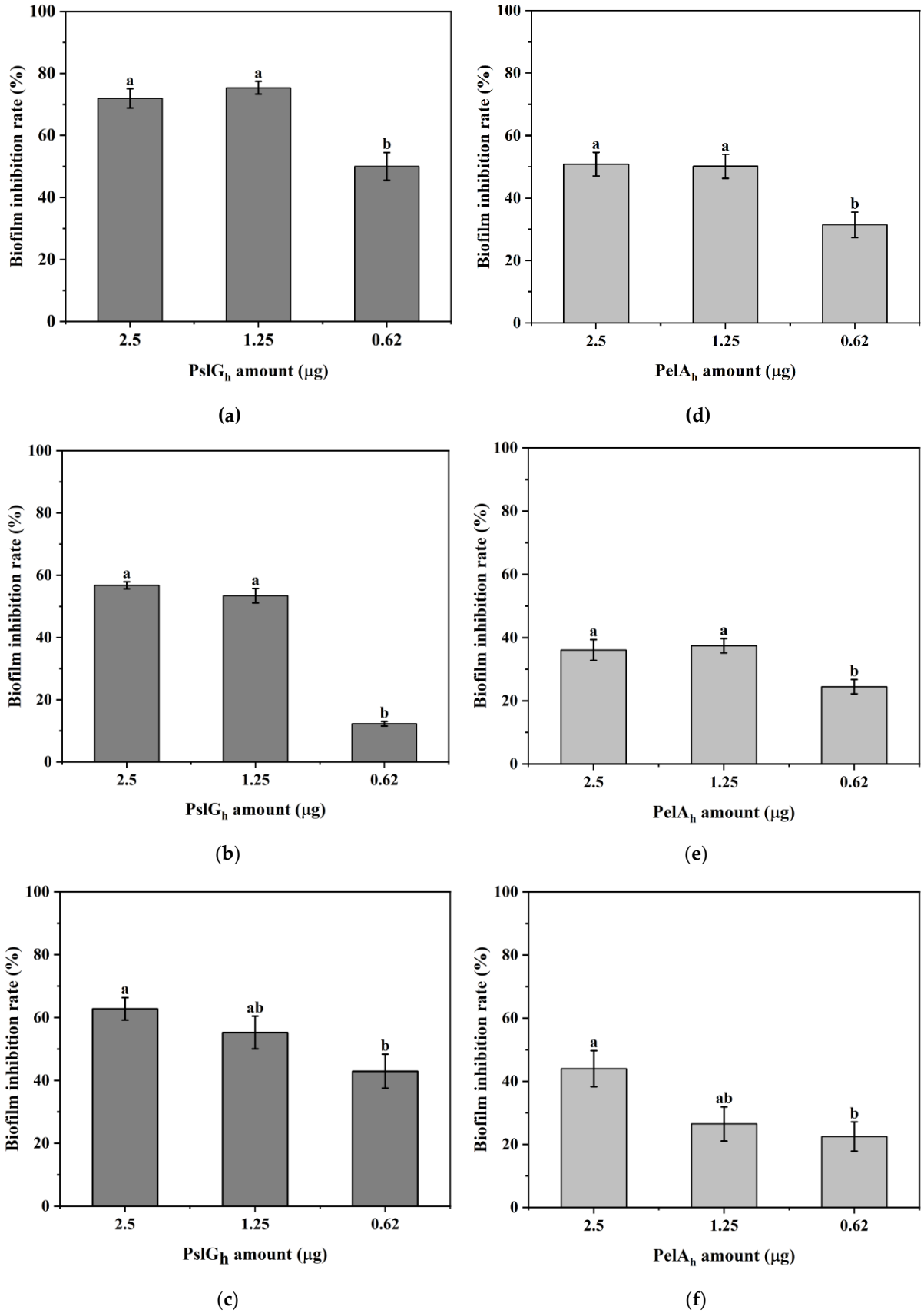

Figure 9. The antibiofilm activity of PelA$_h$ and PslG$_h$ against *P. aeruginosa* PAO-1 biofilm in soluble form (**a**,**d**), immobilized on BC (**b**,**e**), and immobilized on Ar_BC (**c**,**f**). The means with the same superscript are not significantly different, with $p > 0.05$. Error bars represent standard deviation.

4. Conclusions

Bacterial cellulose (BC) is a highly promising biopolymer with a wide range of applications in biomedicine. In this study, we investigated the modification of bacterial cellulose using low-pressure argon plasma to assess its suitability as a carrier for delivering $PelA_h$ and $PslG_h$ proteins, aiming to inhibit the formation of *Pseudomonas aeruginosa* PAO-1 biofilms. Exposure to LPArP strongly influences the structure of bacterial cellulose, converting the surface into a more amorphous form. XPS and ATR-FTIR analyses revealed a significant change in the chemical composition of the BC surfaces, with a reduction in oxygen content and an increase in carbon components. The introduction of a significant number of charged carboxyl groups did not affect the analyzed enzyme's ability to destabilize biofilms. However, the observed structural differences between $PelA_h$ and $PslG_h$ were assumed to be the main reason for the different profiles of their release from modified and nonmodified BC, although the observed differences did not have a significant effect on their antibiofilm activity. Bacterial cellulose modified through exposure to LPArP shows potential for further development as a versatile carrier for delivery systems based on BC. It possesses varying crystallinity and can accommodate proteins with diverse molecular structures, allowing for effective combat against infections caused by biofilm-forming bacteria.

Author Contributions: Conceptualization, M.C. and R.D.; methodology, M.C., E.E., D.M., M.M., M.J.-S. and R.D.; validation, R.D.; formal analysis, R.D.; investigation, M.C., E.E., D.M., M.M. and M.J.-S.; data curation, M.C.; writing—original draft preparation, M.C. and R.D.; writing—review and editing, D.M., M.J.-S. and R.D.; visualization, M.C. and D.M.; supervision, R.D. All authors have read and agreed to the published version of the manuscript.

Funding: This research received no external funding.

Institutional Review Board Statement: Not applicable.

Informed Consent Statement: Not applicable.

Data Availability Statement: The data will be available from the corresponding author on request.

Conflicts of Interest: The authors declare no conflict of interest.

References

1. Hu, S.; Cai, X.; Qu, X.; Yu, B.; Yan, C.; Yang, J.; Li, F.; Zheng, Y.; Shi, X. Preparation of biocompatible wound dressings with long-term antimicrobial activity through covalent bonding of antibiotic agents to natural polymers. *Int. J. Biol. Macromol.* **2019**, *123*, 1320–1330. [CrossRef]
2. Talikowska, M.; Fu, X.; Lisak, G. Application of conducting polymers to wound care and skin tissue engineering: A review. *Biosens. Bioelectron.* **2019**, *135*, 50–63. [CrossRef]
3. Vivcharenko, V.; Przekora, A. Modifications of Wound Dressings with Bioactive Agents to Achieve Improved Pro-Healing Properties. *Appl. Sci.* **2021**, *11*, 4114. [CrossRef]
4. Sulaeva, I.; Henniges, U.; Rosenau, T.; Potthast, A. Bacterial cellulose as a material for wound treatment: Properties and modifications. A review. *Biotechnol. Adv.* **2015**, *33*, 1547–1571. [CrossRef]
5. Cazón, P.; Vázquez, M. Improving bacterial cellulose films by ex-situ and in-situ modifications: A review. *Food Hydrocoll.* **2021**, *113*, 106514. [CrossRef]
6. Wu, S.; Liu, X.; Yeung, A.; Yeung, K.W.K.; Kao, R.Y.T.; Wu, G.; Hu, T.; Xu, Z.; Chu, P.K. Plasma-modified biomaterials for self-antimicrobial applications. *ACS Appl. Mater. Interfaces* **2011**, *3*, 2851–2860. [CrossRef] [PubMed]
7. Stumpf, T.R.; Yang, X.; Zhang, J.; Cao, X. In situ and ex situ modifications of bacterial cellulose for applications in tissue engineering. *Mater. Sci. Eng. C Mater. Biol. Appl.* **2018**, *82*, 372–383. [CrossRef] [PubMed]
8. Szymańska, M.; Hoppe, J.; Dutkiewicz, M.; Sobolewski, P.; Palacz, M.; Janus, E.; Zielińska, B.; Drozd, R. Silicone polyether surfactant enhances bacterial cellulose synthesis and water holding capacity. *Int. J. Biol. Macromol.* **2022**, *208*, 642–653. [CrossRef] [PubMed]
9. Farber, R.; Dabush-Busheri, I.; Chaniel, G.; Rozenfeld, S.; Bormashenko, E.; Multanen, V.; Cahan, R. Biofilm grown on wood waste pretreated with cold low-pressure nitrogen plasma: Utilization for toluene remediation. *Int. Biodeterior. Biodegrad.* **2019**, *139*, 62–69. [CrossRef]
10. Pertile, R.A.; Andrade, F.K.; Alves, C.; Gama, M. Surface modification of bacterial cellulose by nitrogen-containing plasma for improved interaction with cells. *Carbohydr. Polym.* **2010**, *82*, 692–698. [CrossRef]

11. Żywicka, A.; Ciecholewska-Juśko, D.; Szymańska, M.; Drozd, R.; Sobolewski, P.; Junka, A.; Gorgieva, S.; El Fray, M.; Fijałkowski, K. Argon plasma-modified bacterial cellulose filters for protection against respiratory pathogens. *Carbohydr. Polym.* **2023**, *302*, 120322. [CrossRef] [PubMed]
12. Bhanthumnavin, W.; Wanichapichart, P.; Taweepreeda, W.; Sirijarukula, S.; Paosawatyanyong, B. Surface modification of bacterial cellulose membrane by oxygen plasma treatment. *Surf. Coat. Technol.* **2016**, *306*, 272–278. [CrossRef]
13. Mai-Prochnow, A.; Murphy, A.B.; McLean, K.M.; Kong, M.G.; Ostrikov, K.K. Atmospheric pressure plasmas: Infection control and bacterial responses. *Int. J. Antimicrob. Agents* **2014**, *43*, 508–517. [CrossRef] [PubMed]
14. Hagiwara, K.; Hasebe, T.; Hotta, A. Effects of plasma treatments on the controlled drug release from poly(ethylene-co-vinyl acetate). *Surf. Coat. Technol.* **2013**, *216*, 318–323. [CrossRef]
15. Canal, C.; Modic, M.; Cvelbar, U.; Ginebra, M.-P. Regulating the antibiotic drug release from β-tricalcium phosphate ceramics by atmospheric plasma surface engineering. *Biomater. Sci.* **2016**, *4*, 1454–1461. [CrossRef]
16. Kasza, K.; Gurnani, P.; Hardie, K.R.; Cámara, M.; Alexander, C. Challenges and solutions in polymer drug delivery for bacterial biofilm treatment: A tissue-by-tissue account. *Adv. Drug Deliv. Rev.* **2021**, *178*, 113973. [CrossRef]
17. Serra, R.; Grande, R.; Butrico, L.; Rossi, A.; Settimio, U.F.; Caroleo, B.; Amato, B.; Gallelli, L.; de Franciscis, S. Chronic wound infections: The role of *Pseudomonas aeruginosa* and *Staphylococcus aureus*. *Expert Rev. Anti Infect. Ther.* **2015**, *13*, 605–613. [CrossRef]
18. Vanderwoude, J.; Fleming, D.; Azimi, S.; Trivedi, U.; Rumbaugh, K.P.; Diggle, S.P. The evolution of virulence in *Pseudomonas aeruginosa* during chronic wound infection. *Proc. Biol. Sci.* **2020**, *287*, 20202272.
19. Reichhardt, C.; Parsek, M.R. Confocal Laser Scanning Microscopy for Analysis of *Pseudomonas aeruginosa* Biofilm Architecture and Matrix Localization. *Front. Microbiol.* **2019**, *10*, 677. [CrossRef]
20. Azam, M.W.; Khan, A.U. Updates on the pathogenicity status of *Pseudomonas aeruginosa*. *Drug Discov. Today* **2019**, *24*, 350–359. [CrossRef]
21. Al-Wrafy, F.; Brzozowska, E.; Górska, S.; Gamian, A. Pathogenic factors of *Pseudomonas aeruginosa*—The role of biofilm in pathogenicity and as a target for phage therapy. *Postepy Hig. Med. Dosw.* **2017**, *71*, 78–91. [CrossRef] [PubMed]
22. Da Passos Silva, D.; Matwichuk, M.L.; Townsend, D.O.; Reichhardt, C.; Lamba, D.; Wozniak, D.J.; Parsek, M.R. The *Pseudomonas aeruginosa* lectin LecB binds to the exopolysaccharide Psl and stabilizes the biofilm matrix. *Nat. Commun.* **2019**, *10*, 2183. [CrossRef] [PubMed]
23. Baker, P.; Whitfield, G.B.; Hill, P.J.; Little, D.J.; Pestrak, M.J.; Robinson, H.; Wozniak, D.J.; Howell, P.L. Characterization of the *Pseudomonas aeruginosa* Glycoside Hydrolase PslG Reveals That Its Levels Are Critical for Psl Polysaccharide Biosynthesis and Biofilm Formation. *J. Biol. Chem.* **2015**, *290*, 28374–28387. [CrossRef] [PubMed]
24. Vandana; Das, S. Genetic regulation, biosynthesis and applications of extracellular polysaccharides of the biofilm matrix of bacteria. *Carbohydr. Polym.* **2022**, *291*, 119536. [CrossRef]
25. Le Mauff, F.; Razvi, E.; Reichhardt, C.; Sivarajah, P.; Parsek, M.R.; Howell, P.L.; Sheppard, D.C. The Pel polysaccharide is predominantly composed of a dimeric repeat of α-1,4 linked galactosamine and N-acetylgalactosamine. *Commun. Biol.* **2022**, *5*, 502. [CrossRef]
26. Szymańska, M.; Karakulska, J.; Sobolewski, P.; Kowalska, U.; Grygorcewicz, B.; Böttcher, D.; Bornscheuer, U.T.; Drozd, R. Glycoside hydrolase ($PelA_h$) immobilization prevents *Pseudomonas aeruginosa* biofilm formation on cellulose-based wound dressing. *Carbohydr. Polym.* **2020**, *246*, 116625. [CrossRef]
27. Baker, P.; Hill, P.J.; Snarr, B.D.; Alnabelseya, N.; Pestrak, M.J.; Lee, M.J.; Jennings, L.K.; Tam, J.; Melnyk, R.A.; Parsek, M.R.; et al. Exopolysaccharide biosynthetic glycoside hydrolases can be utilized to disrupt and prevent *Pseudomonas aeruginosa* biofilms. *Sci. Adv.* **2016**, *2*, e1501632. [CrossRef]
28. Pestrak, M.J.; Baker, P.; Dellos-Nolan, S.; Hill, P.J.; Da Passos Silva, D.; Silver, H.; Lacdao, I.; Raju, D.; Parsek, M.R.; Wozniak, D.J.; et al. Treatment with the *Pseudomonas aeruginosa* Glycoside Hydrolase PslG Combats Wound Infection by Improving Antibiotic Efficacy and Host Innate Immune Activity. *Antimicrob. Agents Chemother.* **2019**, *63*, e00234-19. [CrossRef]
29. Snarr, B.D.; Baker, P.; Bamford, N.C.; Sato, Y.; Liu, H.; Lehoux, M.; Gravelat, F.N.; Ostapska, H.; Baistrocchi, S.R.; Cerone, R.P.; et al. Microbial glycoside hydrolases as antibiofilm agents with cross-kingdom activity. *Proc. Natl. Acad. Sci. USA* **2017**, *114*, 7124–7129. [CrossRef]
30. Asker, D.; Awad, T.S.; Raju, D.; Sanchez, H.; Lacdao, I.; Gilbert, S.; Sivarajah, P.; Andes, D.R.; Sheppard, D.C.; Howell, P.L.; et al. Preventing *Pseudomonas aeruginosa* Biofilms on Indwelling Catheters by Surface-Bound Enzymes. *ACS Appl. Bio Mater.* **2021**, *4*, 8248–8258. [CrossRef]
31. Asker, D.; Awad, T.S.; Baker, P.; Howell, P.L.; Hatton, B.D. Non-eluting, surface-bound enzymes disrupt surface attachment of bacteria by continuous biofilm polysaccharide degradation. *Biomaterials* **2018**, *167*, 168–176. [CrossRef] [PubMed]
32. Charęza, M.; Przygrodzka, K.; Żywicka, A.; Grygorcewicz, B.; Sobolewski, P.; Mozia, S.; Śmiglak, M.; Drozd, R. Enhancement of Inhibition of the *Pseudomonas* sp. Biofilm Formation on Bacterial Cellulose-Based Wound Dressing by the Combined Action of Alginate Lyase and Gentamicin. *Int. J. Mol. Sci.* **2023**, *24*, 4740. [CrossRef] [PubMed]
33. Beamson, G.; Briggs, D. *High Resolution XPS of Organic Polymers: The Scienta ESCA300 Database*; Wiley: Chichester, UK, 1992; ISBN 0471935921.
34. Przygrodzka, K.; Charęza, M.; Banaszek, A.; Zielińska, B.; Ekiert, E.; Drozd, R. Bacterial Cellulose Production by *Komagateibacter xylinus* with the Use of Enzyme-Degraded Oligo- and Polysaccharides as the Substrates. *Appl. Sci.* **2022**, *12*, 12673. [CrossRef]

35. Jedrzejczak-Silicka, M.; Kordas, M.; Konopacki, M.; Rakoczy, R. Modulation of Cellular Response to Different Parameters of the Rotating Magnetic Field (RMF)-An In Vitro Wound Healing Study. *Int. J. Mol. Sci.* **2021**, *22*, 5785. [CrossRef] [PubMed]
36. Ambrogi, V.; Pietrella, D.; Donnadio, A.; Latterini, L.; Di Michele, A.; Luffarelli, I.; Ricci, M. Biocompatible alginate silica supported silver nanoparticles composite films for wound dressing with antibiofilm activity. *Mater. Sci. Eng. C Mater. Biol. Appl.* **2020**, *112*, 110863. [CrossRef]
37. Drozd, R.; Szymańska, M.; Żywicka, A.; Kowalska, U.; Rakoczy, R.; Kordas, M.; Konopacki, M.; Junka, A.F.; Fijałkowski, K. Exposure to non-continuous rotating magnetic field induces metabolic strain-specific response of *Komagataeibacter xylinus*. *Biochem. Eng. J.* **2021**, *166*, 107855. [CrossRef]
38. Khan, H.; Kadam, A.; Dutt, D. Studies on bacterial cellulose produced by a novel strain of Lactobacillus genus. *Carbohydr. Polym.* **2020**, *229*, 115513. [CrossRef]
39. Abral, H.; Chairani, M.K.; Rizki, M.D.; Mahardika, M.; Handayani, D.; Sugiarti, E.; Muslimin, A.N.; Sapuan, S.M.; Ilyas, R.A. Characterization of compressed bacterial cellulose nanopaper film after exposure to dry and humid conditions. *J. Mater. Res. Technol.* **2021**, *11*, 896–904. [CrossRef]
40. Dayal, M.S.; Goswami, N.; Sahai, A.; Jain, V.; Mathur, G.; Mathur, A. Effect of media components on cell growth and bacterial cellulose production from *Acetobacter aceti* MTCC 2623. *Carbohydr. Polym.* **2013**, *94*, 12–16. [CrossRef]
41. Srikandace, Y.; Apriyana, A.Y.; Zahrad, S.A.; Ramdhani, W.; Asri, P.P.P.; Andriani, D.; Abdullah, A.H.D.; Syampurwadi, A.; Satoto, R.; Karina, M. Bacterial Cellulose Production by *Komagataeibacter xylinus* Using Rice-washed Water and Tofu Processing Wastewater with the Addition of Sodium Glutamate. *Fibers Polym.* **2022**, *23*, 1190–1196. [CrossRef]
42. Chashmejahanbin, M.R.; Salimi, A.; Ershad Langroudi, A. The study of the coating adhesion on PP surface modified in different plasma/acrylic acid solution. *Int. J. Adhes. Adhes.* **2014**, *49*, 44–50. [CrossRef]
43. Hua, Z.Q.; Sitaru, R.; Denes, F.; Young, R.A. Mechanisms of oxygen- and argon-RF-plasma-induced surface chemistry of cellulose. *Plasmas Polym.* **1997**, *2*, 199–224. [CrossRef]
44. Kumar, A.; Singh Negi, Y.; Choudhary, V.; Kant Bhardwaj, N. Characterization of Cellulose Nanocrystals Produced by Acid-Hydrolysis from Sugarcane Bagasse as Agro-Waste. *JMPC* **2020**, *2*, 1–8. [CrossRef]
45. Brassolatti, P.; Kido, H.W.; Bossini, P.S.; Gabbai-Armelin, P.R.; Otterço, A.N.; Almeida-Lopes, L.; Zanardi, L.M.; Napolitano, M.A.; de Da Avó, L.R.S.; Forato, L.A.; et al. Bacterial cellulose membrane used as biological dressings on third-degree burns in rats. *Biomed. Mater. Eng.* **2018**, *29*, 29–42. [CrossRef]
46. Arias, S.L.; Cheng, M.K.; Civantos, A.; Devorkin, J.; Jaramillo, C.; Allain, J.P. Ion-Induced Nanopatterning of Bacterial Cellulose Hydrogels for Biosensing and Anti-Biofouling Interfaces. *ACS Appl. Nano Mater.* **2020**, *3*, 6719–6728. [CrossRef]
47. Tang, S.; Lu, N.; Wang, J.K.; Ryu, S.-K.; Choi, H.-S. Novel Effects of Surface Modification on Activated Carbon Fibers Using a Low Pressure Plasma Treatment. *J. Phys. Chem. C* **2007**, *111*, 1820–1829. [CrossRef]
48. Vasil'kov, A.; Budnikov, A.; Gromovykh, T.; Pigaleva, M.; Sadykova, V.; Arkharova, N.; Naumkin, A. Effect of Bacterial Cellulose Plasma Treatment on the Biological Activity of Ag Nanoparticles Deposited Using Magnetron Deposition. *Polymers* **2022**, *14*, 3907. [CrossRef]
49. Nosworthy, N.J.; McKenzie, D.R.; Bilek, M.M. A new surface for immobilizing and maintaining the function of enzymes in a freeze-dried state. *Biomacromolecules* **2009**, *10*, 2577–2583. [CrossRef]
50. Mensink, M.A.; Frijlink, H.W.; van der Voort Maarschalk, K.; Hinrichs, W.L.J. How sugars protect proteins in the solid state and during drying (review): Mechanisms of stabilization in relation to stress conditions. *Eur. J. Pharm. Biopharm.* **2017**, *114*, 288–295. [CrossRef]
51. Gao, K.; Oerlemans, R.; Groves, M.R. Theory and applications of differential scanning fluorimetry in early-stage drug discovery. *Biophys. Rev.* **2020**, *12*, 85–104. [CrossRef]
52. Pettersen, E.F.; Goddard, T.D.; Huang, C.C.; Couch, G.S.; Greenblatt, D.M.; Meng, E.C.; Ferrin, T.E. UCSF Chimera—A visualization system for exploratory research and analysis. *J. Comput. Chem.* **2004**, *25*, 1605–1612. [CrossRef] [PubMed]
53. Olsson, M.H.M.; Søndergaard, C.R.; Rostkowski, M.; Jensen, J.H. PROPKA3: Consistent Treatment of Internal and Surface Residues in Empirical pKa Predictions. *J. Chem. Theory Comput.* **2011**, *7*, 525–537. [CrossRef] [PubMed]
54. Adepu, S.; Khandelwal, M. Ex-situ modification of bacterial cellulose for immediate and sustained drug release with insights into release mechanism. *Carbohydr. Polym.* **2020**, *249*, 116816. [CrossRef] [PubMed]
55. Jantarat, C.; Muenraya, P.; Srivaro, S.; Nawakitrangsan, A.; Promsornpason, K. Comparison of drug release behavior of bacterial cellulose loaded with ibuprofen and propranolol hydrochloride. *RSC Adv.* **2021**, *11*, 37354–37365. [CrossRef] [PubMed]
56. Colvin, K.M.; Irie, Y.; Tart, C.S.; Urbano, R.; Whitney, J.C.; Ryder, C.; Howell, P.L.; Wozniak, D.J.; Parsek, M.R. The Pel and Psl polysaccharides provide *Pseudomonas aeruginosa* structural redundancy within the biofilm matrix. *Environ. Microbiol.* **2012**, *14*, 1913–1928. [CrossRef]
57. Thi, M.T.T.; Wibowo, D.; Rehm, B.H.A. *Pseudomonas aeruginosa* Biofilms. *Int. J. Mol. Sci.* **2020**, *21*, 8671. [CrossRef]